HiSST: International Conference on
High-Speed Vehicle Science Technology
26–29 November 2018, Moscow, Russia

Numerical Study of Embedded Rocket on Back Pressure Resistance of an RBCC Inlet

Lei Shi[1], Haijian Lou[2], Da Gao[3], Xiaowei Liu[4], Fei Qin[5], Guoqiang He[6]

Abstract

Sufficient back pressure resistance of RBCC inlet is one of the most important performance requirements for an RBCC engine during its whole flight, especially in the near flight duration after the inlet starts at a low Mach number. Higher back pressure resistance of RBCC inlet leads to robust engine operation, more efficient combustion and thus a higher engine thrust and specific impulse. Two-dimensional numerical simulations were conducted based on an RBCC inlet model operating at Mach 2.5. The dynamic generation and movement of the shocks in the inlet were simulated under a certain back pressures. The influence rules of the embedded rocket operation conditions and configuration on the maximum back pressure resistance of the RBCC inlet were also numerically investigated. (1) The embedded rocket significantly increases the back pressure resistance of the inlet by enhancing the total pressure and momentum of the captured flow and sweeping the boundary layer flow near the upper wall. (2) The chamber pressure of embedded rocket influences the maximum back pressure resistance of the RBCC inlet most significantly. The $P_{b,max}$ was effectively enhanced at most by 52.6% when the P_c increased from 0MPa to 9MPa. (3) The influence of the chamber temperature is slight while the expansion angle of rocket nozzle almost had no effect on the back pressure resistance.

Key words: RBCC, inlet, back pressure resistance, embedded rocket, numerical simulation

Nomenclature

M – Mach number
P – pressure, MPa, Pa
T – temperature, K
v – velocity, m/s
E – momentum, kg·m/s
θ – apex angle of embedded rocket nozzle, degree
x – x coordinate, mm
y – y coordinate, mm
Δ – throttle ratio of 2-D supersonic inlet, %
h – isolator height, mm
H – combustor height, mm

Subscripts
b – back pressure
c – embedded rocket chamber
0 – total
∞ – free incoming flow
max - maximum

1. Introduction

A rocket-based combined-cycle (RBCC) engine combines a rocket engine and an air-breathing engine in one single flowpath, and has both the advantages of high thrust-to-weight ratio of the rocket engine and high specific impulse of the air-breathing engine[1]. It can take off from the ground, accelerate and climb through multiple modes until enter into orbit. The simple structural, reusable and highly safe propulsion system achieves a good combination of economy and efficiency. Therefore, RBCC engine is one of the most prospective approaches to realize reusable orbit transportations and hypersonic cruises[2].

[1] *Northwestern Polytechnical University, P. R. China, shilei@nwpu.edu.cn*
[2] *Northwestern Polytechnical University, P. R. China, 2013300673@mail.nwpu.edu.cn*
[3] *Northwestern Polytechnical University, P. R. China, gaoda@mail.nwpu.edu.cn*
[4] *Northwestern Polytechnical University, P. R. China, xiaowei420@aliyun.com*
[5] *Northwestern Polytechnical University, P. R. China, qinfei@nwpu.edu.cn*
[6] *Northwestern Polytechnical University, P. R. China, gghe@nwpu.edu.cn*

An inlet plays a vital role in any air-breathing engine. Favorable start ability, good mass capture and total pressure recovery capabilities, as well as high back pressure resistance are commonly required. Specially, an RBCC inlet should possess even better comprehensive performance than a common supersonic inlet since it commonly operates through various modes in a wide flight range that includes static, subsonic, transonic, supersonic and hypersonic flight regimes. Commonly, an RBCC inlet must start at a relatively low Mach number since if the start Mach number is too high, the RBCC engine will operate in the ejector mode for a longer duration, and correspondingly, the comprehensive engine performance (for instance, the average specific impulse) along the whole flight trajectory will be seriously impacted. However, if the RBCC inlet starts at a low Mach number, its back pressure resistance is relatively weak, especially in the near flight duration after it starts, the inlet easily falls into unstart state resulted from the combustion in the combustor. Therefore, how to enhance the back pressure resistance of an RBCC inlet becomes an important issue in the RBCC engine study.

There are several studies conducted on the back pressure resistance of supersonic inlets. For instance, Liang et al. studied the characteristics of shock string in the isolator of a supersonic inlet and proposed the concept of "maximum working back pressure"[3]. As for RBCC inlets, there are also some relevant research results. Liu investigated the influence of the inlet height and sidewall contraction ratio on the start performance. The conclusion was draw that an RBCC inlet with appropriate geometries could operate well in a wide Mach number range[4,5]. In order to further improve the inlet performance in ejector and ramjet modes, a variable geometry two-dimensional inlet scheme, combining the internal contraction ratio adjustment and the boundary layer flow control was presented. Results showed that the variable geometry scheme effectively decreased the start Mach number and inlet drag, and increased the total pressure recovery coefficient[6]. Liu et al. found the ejector effect of rocket could improve the back pressure resistance of the RBCC inlet significantly when the rocket plume was over-expanded[7]. However, the detailed mechanism and the influence rules of the embedded rocket on the back pressure resistance of the RBCC inlet were not studied.

In this case, the embedded rocket plume with high momentum can be fully taken use of to improve the back pressure resistance of an RBCC inlet. Nevertheless, the inherent function mechanism and the influence rules of the rocket parameters on the back pressure resistance should be clarified. The associating studies were numerically conducted in this paper. Although the actual structure of the engine and the internal flowfields are three-dimensional, two-dimensional numerical simulations were employed in the paper in full consideration of computation efficiency.

2. Numerical methods and validations

2.1. Numerical methods

All the calculations were carried out by FLUENT software in this paper. 2-D Detached Eddy Simulation (DES) governing equations were chosen, which exhibits high accuracy in transient simulations. Roe model was employed to describe convection processes.

The governing equations are as following:

$$\frac{\partial \rho}{\partial t} + div(\rho \vec{u}) = 0 \tag{1}$$

$$\frac{\partial(\rho u)}{\partial t} + div(\rho u \vec{u}) = div(\mu \cdot gradu) - \frac{\partial p}{\partial x} + S_{Mx} \tag{2}$$

$$\frac{\partial(\rho v)}{\partial t} + div(\rho v \vec{u}) = div(\mu \cdot gradv) - \frac{\partial p}{\partial y} + S_{My} \tag{3}$$

$$\frac{\partial(\rho i)}{\partial t} + div(\rho i \vec{u}) = div(\lambda \cdot gradT) - p \cdot div(\vec{u}) + \Phi + S_i \tag{4}$$

Equations (1) ~ (4) are respectively the continuity equation, momentum conservation equation and energy conservation equation. And Φ is expressed as following:

$$\Phi=\mu\left\{2\left[\left(\frac{\partial u}{\partial x}\right)^2+\left(\frac{\partial v}{\partial y}\right)^2\right]+\left(\frac{\partial u}{\partial y}+\frac{\partial v}{\partial x}\right)^2\right\}+\lambda\left(div\vec{u}\right)^2 \tag{5}$$

u,v,w---x,y,z component of the velocity;

ρ---density ;

μ---kinetic viscosity;

i---internal energy;

λ---coefficient of thermal conductivity;

T---temperature;

p---pressure;

S_{Mx}, S_{Mv} ---fluid sources;

S_i ---heat source.

DES method combines Reynolds-Averaged Navier-Stokes (RANS) technology in the attached boundary layers and the Large-Eddy Simulation (LES) technology in the separated regions[8,9]. It has the advantages of the high efficiency of RANS and the high accuracy of LES in the complicated flowfield. Xue validated the DES method in the simulation of the RBCC combustion flowfield[10]. Under conditions of different flowpath configurations and different rocket operation status, the DES method shows high accuracy in the characteristic of the combustion flowfield.

2.2. Numerical validations

The detailed results of experiments performed on internal flow fields in a typical 2-D supersonic inlet were used as the numerical validation reference[11]. The inlet in Fig.1 within the throat length as 79.3mm and Δ as 0% that operated at M_∞=2.5 was chosen as the validation object.

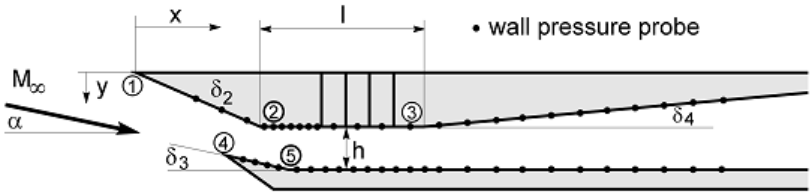

Inner width of the intake:	52mm
channel height h:	15mm
total length:	400mm
incidence angle of the main flow α:	10°
second ramp angle δ_2:	21,5°
first lip angle δ_3:	9,5°
isolator divergence angle δ_4:	5°

location acc. to Fig. 3	x [mm]	y [mm]
1	0	0
2	45,7	18,0
3	75,0-145,0 (step 10)	18,0
4	35,0	29,0
5	58,9	33,0

Fig.1 2-D supersonic inlet model for numerical validations[11]

The computational meshes and boundary condition settings are illustrated in Fig.2. All the grids were structural, while the size was less than 0.5mm. Boundary layer refinements to the walls and local grid refinements near the ramp's turn and entrance were adopted to facilitate the calculation of viscous effects and shock capture. In the calculations, if all the residuals of the equations drop to less than 10^{-3}, while the relative in/out mass flow rate drops under 10^{-4} stably, the results are considered to be converged. Additionally, no slip adiabatic walls were employed in the inlet.

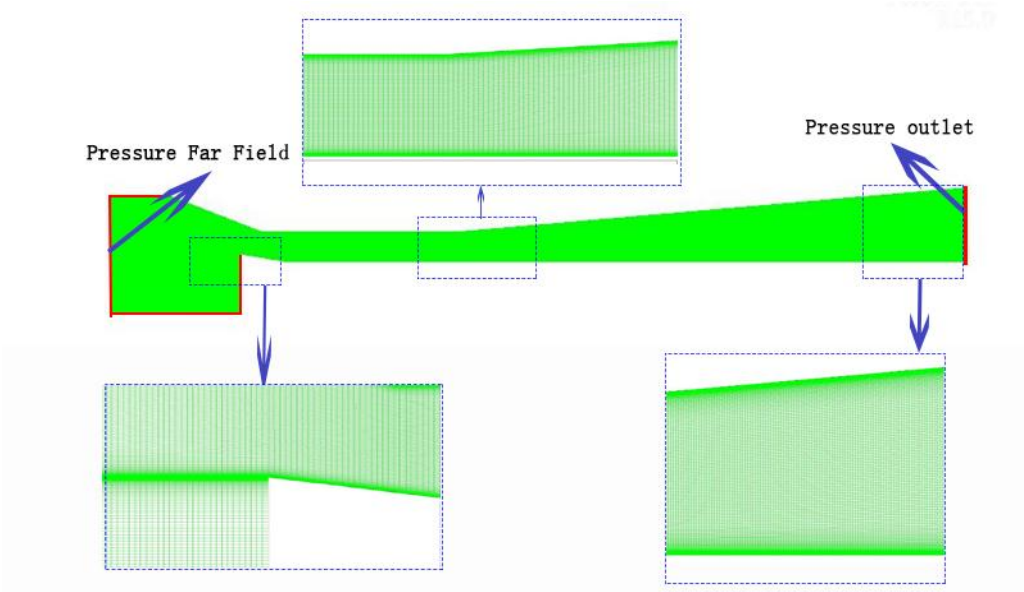

Fig.2 Computational meshes and boundary condition settings for RBCC inlet

A diagram of the internal flow in the inlet and a schlieren image obtained in the freejet tests are shown in Fig.3, while the y^+ distributions along the walls and Mach contours in the inlet obtained in the numerical simulations are shown in Fig.4 as well. These figures confirm the reasonability and credibility of the employed numerical methods in this paper.

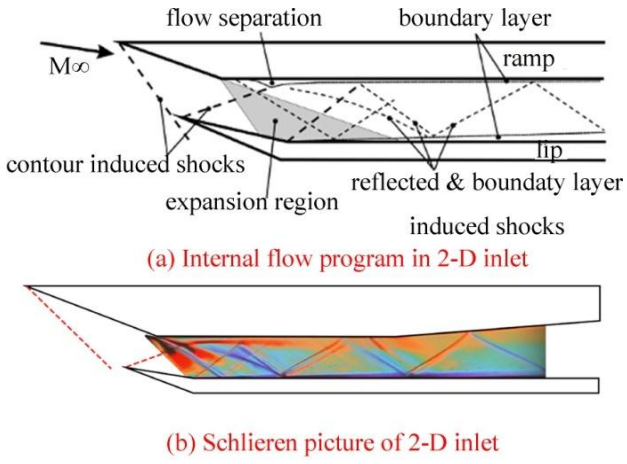

Fig.3 Test results[11]

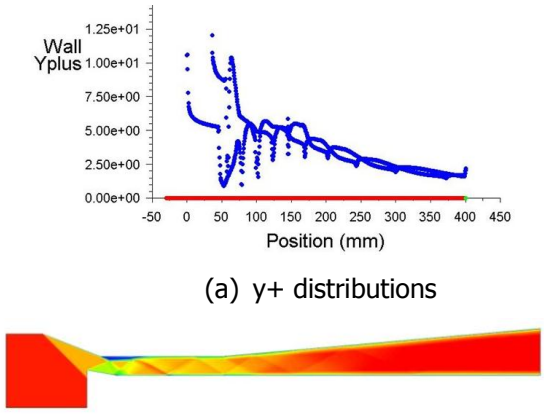

Fig.4 Numerical results

3. RBCC inlet configuration

The RBCC inlet model employed in this paper was established through some modifications on the 2-D supersonic inlet model for numerical validations. As Fig.5 illustrated, the divergence section was replaced by a step along with a straight section. The step was adopted for implementation of the embedded rocket, while the straight section acted as a mixing section for the RBCC engine.

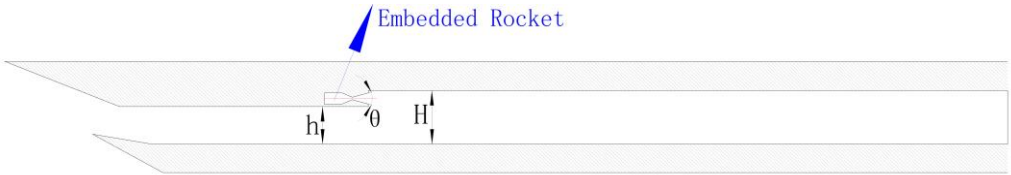

Fig.5 RBCC inlet model

The inlet geometry parameters were as follows:

- The length of the whole inlet kept as 400mm.
- The isolator height (h) was 15mm.
- The ramp angle and the lip angle were kept the same as before: 21.5° and 9.5°respectively.

A rocket was embedded at the step：

- The height of the step was 0.3H.
- The expansion ratio of the rocket nozzle was 8.
- The apex angle of the convergent section was 45°.
- The divergent angle (θ) of the rocket nozzle was variable in the study, which was selected as 15°, 30° and 45° respectively.

4. Results and discussions

Several different cases were numerically calculated. The influences of three key parameters of the embedded rocket on the back pressure resistance were mainly focused on: P_c, T_c representing mixing ratio, and θ. The variations of these parameters in the simulations are listed in Tab.1.

Table 1. Parameter settings of embedded rocket in numerical simulations

No.	P_c	T_c	θ
1	/	2000	30
2	3	2000	30
3	6	2000	30
4	9	2000	30
5	9	1000	30
6	9	3000	30
7	9	2000	15
8	9	2000	45

In the No.1 case, the RBCC inlet functioned without operation of the embedded rocket. The corresponding maximum back pressure resistance was calculated as 0.19MPa.

4.1. Operational characteristics in RBCC inlet under a certain back pressure

When the embedded rocket did not operate, the RBCC inlet functioned in the same way as a common supersonic inlet. The interior flowfield and the dynamic developing process of the waves in the inlet under the certain back pressure of 0.19MPa are shown in Fig.6. Under the condition of P_b= 0MPa, the RBCC inlet started smoothly. The oblique shocks established at the ramp wall and the cowl lip, while the expansion waves formed at the shoulder, and they reflected continuously in the isolator. Then an obvious expansion wave formed at the step and reflected downstream along the duct. As the back pressure functioned, the pre-combustion shocks along with the separation bubbles formed in the isolator and moved upstream continuously till they stood at a position near the cowl lip at 9ms approximately. In this case, the maximum back pressure resistance of the RBCC inlet was limited as 0.19MPa.

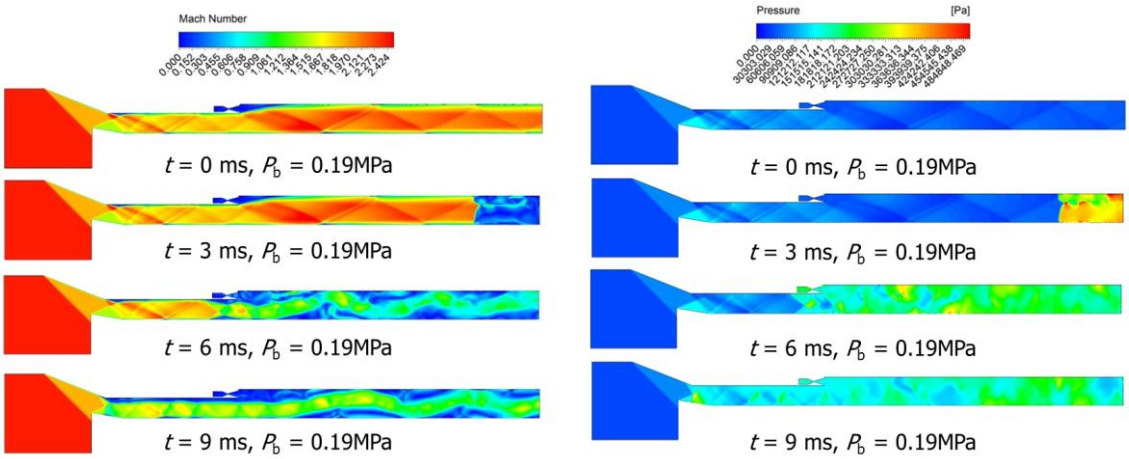

(a) Pressure contours (b) Mach contours

Fig.6 Dynamic moving process of the shock trains in the inlet at P_b= 0.19MPa

However, the interior flowfields in the RBCC inlet changed greatly as the embedded rocket operating. In Fig.7, as the rocket chamber pressure increased, the pre-combustion shocks along with the boundary layer separations in the isolator moved downstream obviously. As well, the pressure and Mach number distributions along the RBCC inlet in Fig.8 also reflect the movement of the shocks intuitively. The higher the rocket chamber pressure was, the better the enhancement on the back pressure resistance of the RBCC inlet performed.

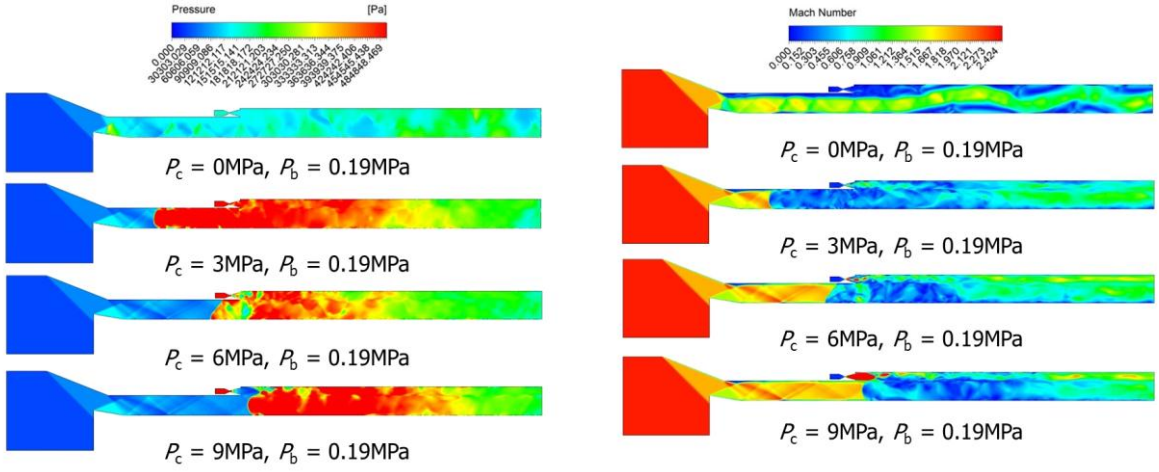

(a) Pressure contours (b) Mach contours

Fig.7 Flowfields in RBCC inlet under different P_c at P_b= 0.19MPa

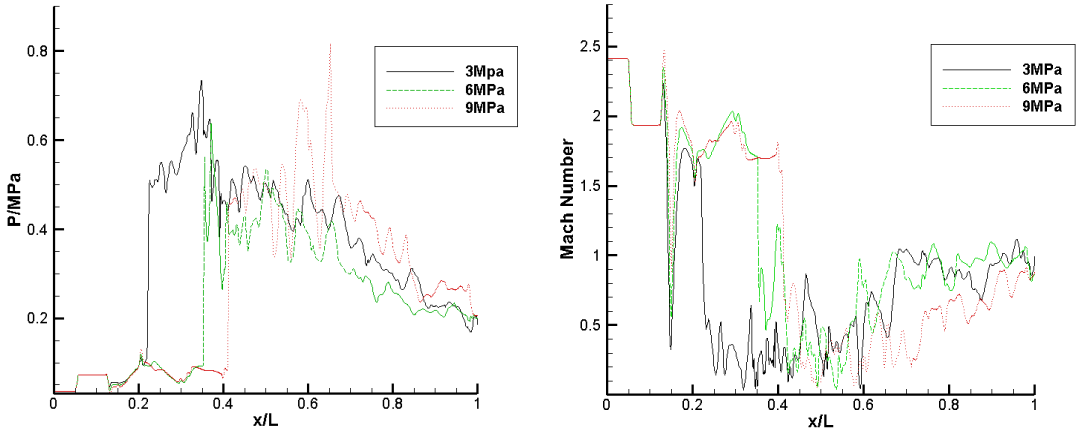

(a) Pressure distributions (b) Mach number distributions

Fig.8 Pressure and Mach distributions along RBCC inlet under different P_c at P_b= 0.19MPa

This indicated that the embedded rocket had a significant influence on the operational characteristics in the RBCC inlet under a certain back pressure. Its plume within high momentum and energy greatly improved the back pressure resistance of the RBCC inlet. On one hand, as Tab.2 listed, the rocket plume improved the quality of the captured flow by effectively enhancing its inherent total pressure and momentum. On the other hand, the rocket plume swept the boundary layer flow near the upper wall, and correspondingly, inhibited or delayed the reverse spread of the serious separation in the boundary layer induced by the high combustion pressure.

Table 2. Key parameters near exit of RBCC inlet under different P_c at P_b= 0.19MPa

P_c/MPa	P_0/Pa	E/(kg·m/s)
/	301926.75	5100.672
3	522278.69	6818.809
6	874412.25	8725.711
9	1259128	10361.590

4.2. Influence rules of embedded rocket on back pressure resistance of RBCC inlet

The influence rules of embedded rocket operation conditions and its configuration on the maximum back pressure resistance of the RBCC inlet were also numerically investigated.

The maximum back pressure resistance under different P_c was numerically obtained respectively, which is shown in Fig.9. With the rocket chamber pressure increasing, the mixing effect between the captured air and the rocket plume was highly enhanced while the momentum and energy transfer were greatly intensified. The quality of the captured flow was thus improved and the back pressure resistance was significantly increased. The calculated results showed that $P_{b,max}$ was highly increased by 52.6% when P_c = 9MPa, compared to that at P_c = 0MPa.

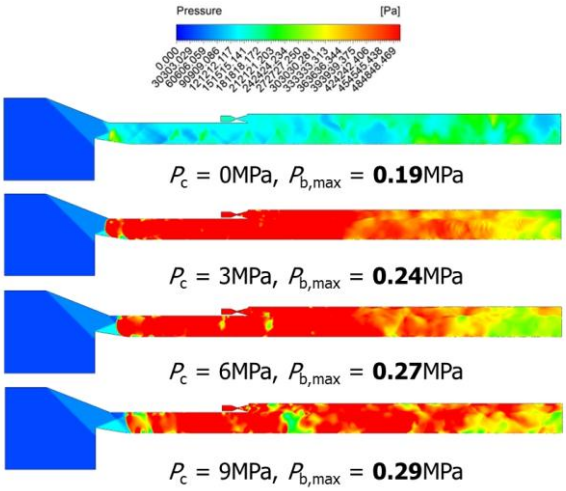

Fig.9 Pressure contours in RBCC inlet under different P_c at corresponding $P_{b,max}$

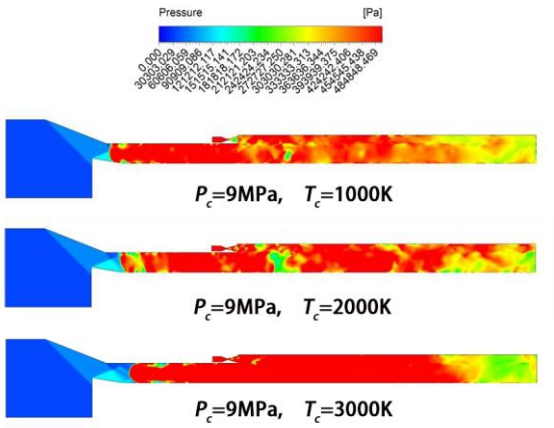

Fig.10 Pressure contours in RBCC inlet under different T_c at P_c= 9MPa & P_b= 0.29MPa

Table 3. Key parameters near exit of RBCC inlet under different T_c at P_c= 9MPa & P_b= 0.29MPa

T_c/K	P_0/Pa	V/(m/s)	E/(kg.m/s)
1000	1118699	735.2573	10280.073
2000	1259128	741.08759	10361.590
3000	1387263	749.1123	10473.789

Another parameter analyzed in the paper was the rocket chamber temperature. Under the same condition of P_c= 9MPa, T_c varied from 1000K to 3000K. As Fig.10 shows, the influence of the temperature on the back pressure resistance was not significant. As T_c increased, the pre-combustion shocks moved downstream slightly, which meant that the back pressure resistance of the RBCC inlet was slightly enhanced. Based on the parameters in Tab.3, the reason was that the plume with high temperature enhanced the total pressure and the momentum of the captured flow by a certain degree and thus improved its quality.

The apex angles of the rocket nozzle were finally analyzed in the study and the results are shown in Fig.11 and Tab.4. Although the flowfield in the inlet changed somewhat when the apex angle of the rocket nozzle varied, the key parameters such as the total pressure and the momentum of the captured flow were almost not changed, and correspondingly, the pre-combustion shocks almost maintained at the same position in the inlet. These indicated that the apex angles of the rocket nozzle almost had no effect on $P_{b,max}$.

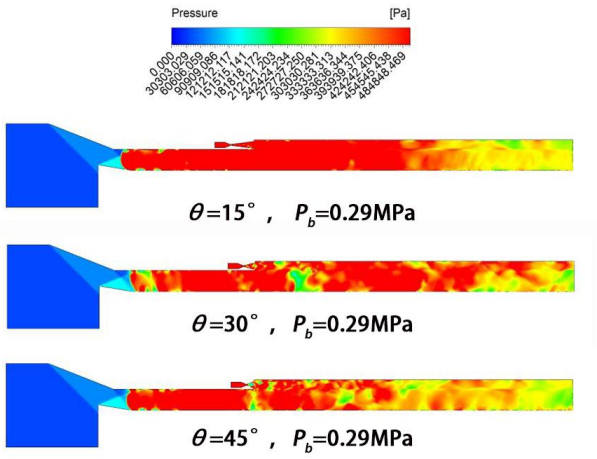

Fig.11 Pressure contours in RBCC inlet within different θ at P_c**= 9MPa &** P_b**= 0.29MPa**

Table 4. Key parameters near exit of RBCC inlet within different θ at P_c= 9MPa & P_b= 0.29MPa

θ/°	P_0/Pa	V/(m/s)	E/(kg.m/s)
15	1323676.1	750.44	10492.352
30	1259128	741.08759	10361.590
45	1346453.8	748.8	10469.422

5. Conclusion

Numerical studies were conducted based on a typical two-dimensional RBCC inlet which operated at Mach 2.5. The influence rules of the embedded rocket on the back pressure resistance were obtained. Some conclusions are as follows:

(1) An RBCC inlet must start at a relatively low Mach number in full consideration of the whole flight trajectory of the RBCC engine. However, in this case, the back pressure resistance of the inlet is relatively weak, especially in the near flight duration after it starts, the inlet easily falls into unstart state resulted from the combustion in the combustor. Therefore, to enhance the back pressure resistance of an RBCC inlet effectively becomes an important issue in the RBCC engine study.

(2) The embedded rocket can significantly improve the back pressure resistance of the inlet. The rocket plume enhances the total pressure and momentum of the captured flow and sweeps the boundary layer flow near the upper wall, which effectively inhibits or delays the reverse spread of the serious separation in the boundary layer.

(3) The chamber pressure of the embedded rocket significantly influences the back pressure resistance of the RBCC inlet. The $P_{b,max}$ is greatly enhanced by 52.6% when the P_c changes from 0MPa to 9MPa in this paper.

(4) The influences of the chamber temperature and the apex angle of the rocket nozzle on the back pressure resistance of the RBCC inlet are much weaker. As T_c increases from 1000K to 3000K, the pre-combustion shocks moves downstream slightly due to a little enhancement of the total pressure and momentum of the captured air. The apex angle of the rocket nozzle has almost no effect on $P_{b,max}$.

Acknowledgment

This work was financially supported by the National Natural Science Foundation of China through grant 51606156.

References

1. A. Siebenhaar, M. Bulman. The Strutjet Engine: The Overlooked Option for Space Launch. AIAA 1995-3124.
2. T. Fujikawa, T. Tsuchiya, S. Tomioka. Multi-Objective, Multidisciplinary Design Optimization of TSTO Space Planes with RBCC Engines. AIAA 2015-0650.
3. Dewang Liang, Bo Li. Back pressure propagation mode and maximum working back pressure of hypersonic inlet isolator. Acta Aerodynamica Sinica,2006(04):454-460.(in Chinese)
4. Xiaowei Liu. Investigation of Wide Applicability Inlet for RBCC Power. Northwestern Polytechnical University, Xi'an, China, 2002. (in Chinese)
5. Xiaowei Liu, Guoqiang He, Peijin Liu. Numerical Investigation of Starting Characteristics for RBCC Supersonic Sidewall-compression Inlets.AIAA 2009-5225.

6. Xiaowei Liu, Guoqiang He, Peijin Liu. Investigation of a RBCC 2D variable geometry inlet scheme. Journal of Solid Rocket Technology, 2010,33(04):409-413+418.(in Chinese)
7. Da Liu, Bo Li, Guoping Huang. Rocket jet effect on the performance of an RBCC inlet. Journal of Propulsion Technology, 2010, 31(02):153-160.
8. Strelets M. Detached eddy simulation of massively separated flows. AIAA 2001-0879.
9. Scott M. DES and BANS simulations of delta wing vortical flows. AIAA 2002-0587.
10. Rui Xue. Investigation on the Flow Characteristic of the RBCC Isolator and the Interaction with the Combustor. Northwestern Polytechnical University, Xi'an, China, 2016. (in Chinese)
11. Herrmann C, Koschel W. Experimental Investigation of the Internal Compression inside a Hypersonic Intake. AIAA 2002-4130.